A Topology-Optimized Approach to Material-Efficient Mechanical Component Design Using Additive Manufacturing

K Sri Harsha Reddy[1], K Durga Rao[2], B Lakshmi[3], M Sindhu[4]
[1,2,3]*Assistant Professor, Department of Mechanical Engineering, University College of Engineering, Adikavi Nannaya University*
[4]*Student, Department of Mechanical Engineering, University College of Engineering, Adikavi Nannaya University*

***Abstract*—Additive Manufacturing (AM) offers unprecedented flexibility in producing lightweight, geometrically complex mechanical components that are often unattainable through conventional fabrication routes. This study proposes a comprehensive topology-optimization–driven design framework tailored specifically for AM-enabled mechanical structures, with the objective of maximizing material efficiency while maintaining high structural performance. The methodology begins with the formulation of functional and operational requirements such as load-bearing capability, stiffness criteria, and application-specific constraints followed by the development of an initial CAD model that incorporates AM process limitations, including build orientation, minimum feature size, and support-structure considerations.**

Topology optimization is then employed to strategically eliminate low-stress material regions while preserving manufacturability and global structural integrity. The optimized geometry is subsequently validated using finite element analysis (FEA) under realistic loading scenarios, explicitly accounting for AM-related factors such as anisotropic material behavior, process-induced variability, and post-processing influences.

Results demonstrate that the proposed approach achieves significant reductions in material usage without compromising mechanical reliability, underscoring the value of integrating topology optimization with AM-centric design practices. This work highlights the potential of AM-driven optimization strategies in advancing sustainable, high-performance mechanical component development.

***Index Terms*—Additive Manufacturing, Topology Optimization, Lightweight Structures, Finite Element Analysis, Structural Reliability, Material Efficiency.**

I. INTRODUCTION

The rapid growth of urban populations and the corresponding demand for sustainable food production have accelerated the adoption of soilless cultivation systems such as hydroponics [1-2]. Hydroponic technologies reduce water consumption, increase crop yield, and allow cultivation in space-limited environments, making them well-suited for modern urban agriculture [3-4]. The historical roots of hydroponics can be traced back to early civilizations, including the Hanging Gardens of Babylon and the floating gardens of the Aztecs [5], while contemporary systems have evolved into modular high-density vertical farming infrastructures [6-7]. Among these, hydroponic towers have emerged as a compact and efficient vertical farming solution capable of continuous nutrient delivery and year-round production [8-9]. However, traditional hydroponic tower components often face challenges related to bulkiness, non-optimized form, material wastage, and limited adaptability to varied environmental constraints [10-11].

Additive Manufacturing (AM) is increasingly recognized as a viable method for addressing these design limitations by enabling the fabrication of intricate, lightweight, and application-specific structures that cannot be achieved through conventional subtractive manufacturing methods [12-13]. AM offers unique advantages in producing customized agricultural system components with reduced material consumption, improved performance, and enhanced geometric freedom [14].

When combined with topology optimization, AM facilitates the systematic removal of low-stress regions, resulting in high-strength yet material-efficient structures suitable for demanding applications such as hydroponic towers subjected to multi-directional loads, fluid-induced stresses, and environmental variability [15-16].

Design for Additive Manufacturing (DfAM) further incorporates process-specific constraints including minimum feature size, anisotropic behavior, build orientation, and support-structure requirements to ensure manufacturability and structural integrity [17-18]. Finite Element Analysis (FEA) provides an essential validation step, enabling accurate assessment of optimized designs under realistic operational conditions [19]. Recent studies also highlight the importance of accounting for AM-specific defects, thermal-gradient-induced distortions, and post-processing effects to ensure long-term functional performance [20-21].

Integrating these methodologies provides a promising pathway for developing next-generation hydroponic tower components that are lighter, stronger, and more resource-efficient. Such advancements align with global sustainability priorities and the increasing emphasis on resilient food production systems capable of scaling within dense urban environments [22-23]. Accordingly, this research proposes a topology-optimized, AM-driven design framework aimed at enhancing the material efficiency, mechanical reliability, and functional adaptability of hydroponic tower components. The presented work demonstrates the synergistic benefits of combining AM with advanced structural optimization techniques to support the future of sustainable vertical agriculture.

II. METHODOLOGY

The methodology adopted in this study follows a systematic workflow integrating design formulation, topology optimization, material selection, simulation and performance validation.

2.1 Design Development and Topology Optimization

The work begins with a comprehensive review of existing hydroponic systems, AM technologies, and sustainable materials to establish key design parameters such as modularity, structural stability, water-flow efficiency, and printability constraints. Based on these requirements, a detailed 3D CAD model of the hydroponic tower is created in SOLIDWORKS, incorporating essential components including the tower column, pots, and internal water-distribution channels as shown in Fig. 2.1 to Fig. 2.5 Topology-optimization techniques are then applied to identify and remove low-stress material regions while ensuring sufficient load-bearing capability. Iterative modifications to the CAD model are performed to balance mechanical performance, weight reduction, and manufacturability.

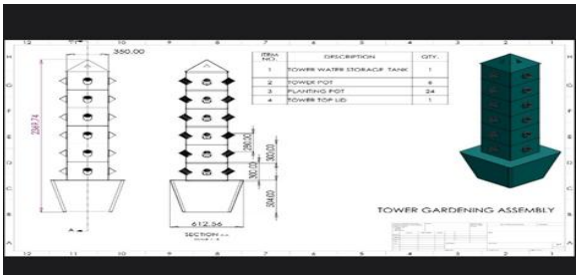

Fig. 2.1 Shows the Hydroponic Tower Design

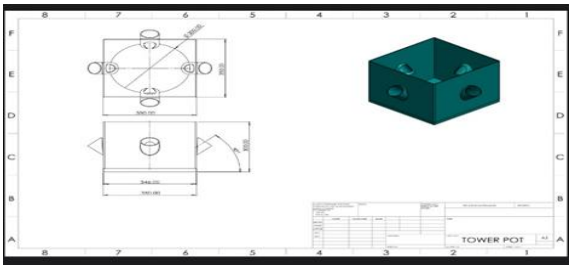

Fig. 2.2 shows the Design parameters of Tower Pot

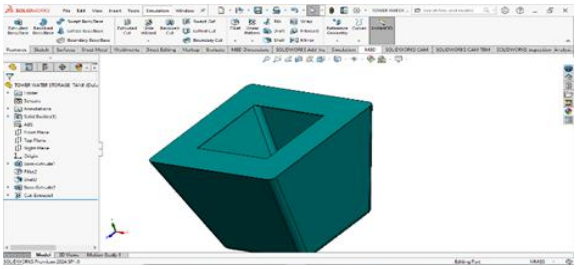

Fig. 2.3 shows the design of Tower Water Storage Tank

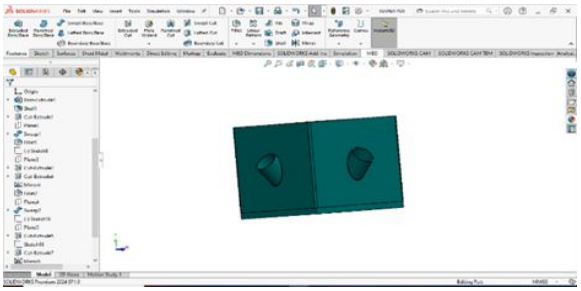

Fig. 2.4 shows the Design of Tower Pot

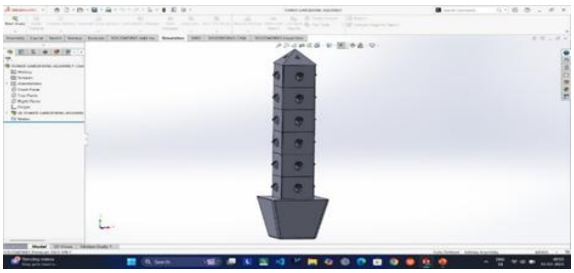

Fig. 2.5 Shows the Design of Hydroponic Tower Assembly

2.2 Material Selection and Property Definition

Acrylonitrile Butadiene Styrene (ABS) is selected as the primary material due to its high impact resistance, thermal stability, smooth surface finish, and suitability for complex 3D-printed geometries. Limitations such as UV sensitivity and non-biodegradability are also considered. The mechanical and thermal properties of ABS used for the simulation phase including elastic modulus, density, and tensile strength are summarized in Table 2.1

Table 2.1 shows the properties of material		
Property	Value	Units
Elastic Modulus	$2x10^9$	N/m^2
Poisson's Ratio	0.394	N/A
Shear Modulus	$318.9x10^6$	N/m^2
Mass Density	1020	Kg/m^3
Tensile Strength	$30x10^6$	N/m^2
Thermal Conductivity	0.2256	W/(m.K)
Specific Heat	1386	J/(kg.K)

2.3 Simulation and Performance Evaluation

Structural evaluation of the optimized design is conducted using SOLIDWORKS Simulation. The CAD geometry is assigned the ABS material properties (Fig. 2.6), and appropriate boundary conditions such as fixed supports and water-weight loads are applied (Fig. 2.7). A refined mesh is generated using Jacobian-based controls as shown in Fig. 2.8

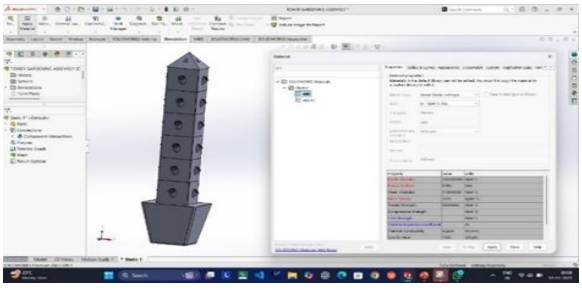

Fig. 2.6 shows the Material Assigning

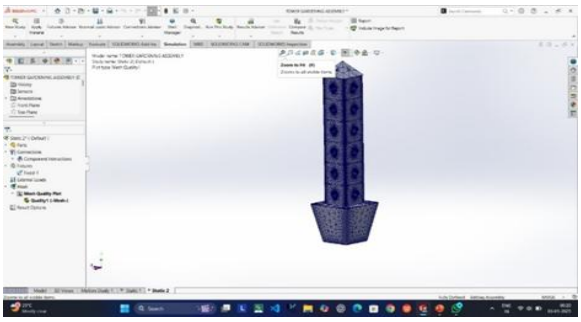

Fig. 2.7 shows the Applied boundary conditions

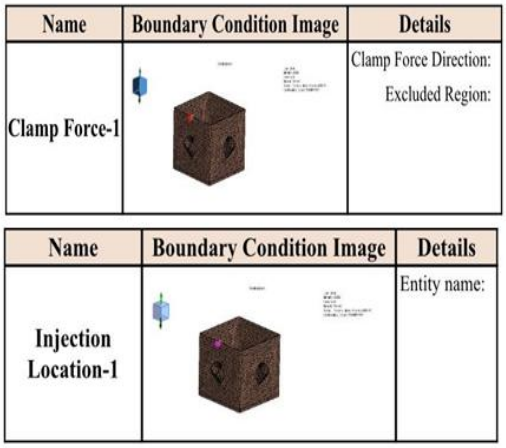

Fig. 2.8 Shows the Meshing of Hydroponic Tower

Static structural analysis is performed to solve the governing equation $[K]\{u\} = \{F\}$, where [K] is the global stiffness matrix, {u} represents the unknown nodal values, and {F} is the force or load vector, yielding displacement, stress, and strain distributions across the tower. Post-processing involves examining contour plots, deformation fields, and factor-of-safety values to identify critical stress paths and potential failure regions. These insights guide final design improvements.

Additional studies include thermal analysis to evaluate temperature gradients and thermal stresses, and CFD analysis to assess water-flow behavior, pressure distribution, and nutrient delivery efficiency. These simulations collectively ensure the hydroponic tower performs reliably under structural, thermal, and fluid-dynamic conditions.

2.3.1 Prototyping and Experimental Validation

Once validated through simulation, the optimized tower components are fabricated using Fused Deposition Modeling (FDM) with ABS filament.

Printing parameters such as layer thickness, infill density, and build orientation are selected to maximize structural reliability.

II. RESULTS AND DISCUSSION

The performance of the topology-optimized hydroponic tower component was evaluated through numerical simulations, focusing primarily on mold-flow behavior, pressure distribution, shear characteristics, temperature uniformity, and packing-phase stability. The results provide insight into manufacturability, structural consistency, and the suitability of the selected ABS material for additive manufacturing and molding processes. The analysis outcomes are categorized into Fill Results and Pack Results, as illustrated through the visual outputs in Fig. 3.1 to Fig. 3.9

3.1 Fill Stage Analysis

The fill stage represents the initial material flow during mold filling. Four major parameters pressure, fill time, flow-front temperature, and shear rate were analyzed to assess flow uniformity and defect formation tendencies.

(i) Pressure at End of Fill: The distribution of internal cavity pressure at the end of filling is shown in Fig. 3.1. The pressure ranged from 0 MPa to 74.59 MPa, indicating that specific regions near constricted flow paths required significantly higher pressure to achieve complete filling. A maximum filling pressure of 74 MPa is acceptable for ABS molding, but the concentration of high-pressure zones suggests potential refinement of gate placement or flow channel geometry to reduce resistance and improve uniformity.

(ii) Fill Time Distribution: The total fill time for the part is presented in Fig. 3.2, with values ranging between 0.00514 sec and 3.847 sec. The color gradient shows that areas closest to the gate fill rapidly, while outer corners and thin-walled regions exhibit longer fill times. Although complete filling is achieved without short-shot defects, the delayed fill regions may cause uneven molecular orientation or inconsistent packing.

(iii) Flow Front Central Temperature: The temperature distribution at the advancing flow front is illustrated in Fig. 3.3, showing a narrow temperature range of 265.15°C to 268.70°C. The uniform temperature profile indicates stable thermal conditions throughout filling, minimizing risks of premature solidification, cold weld lines, and surface defects. However, high central temperatures can elevate shear-heating effects in narrow sections. (iv) Shear Rate at End of Fill: The shear rate distribution shown in Fig. 3.4 ranges from 3.33 s^{-1} to 41,529 s^{-1}. Extremely high shear rates near gates and sharp corners may lead to polymer chain degradation, adversely affecting strength and surface finish. Flow channel smoothing or injection-speed adjustments may be required.

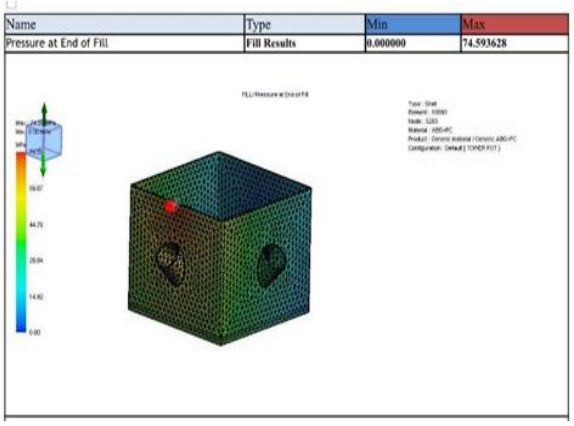

Fig. 3.1 shows the Pressure at end of Fill (Top Right)

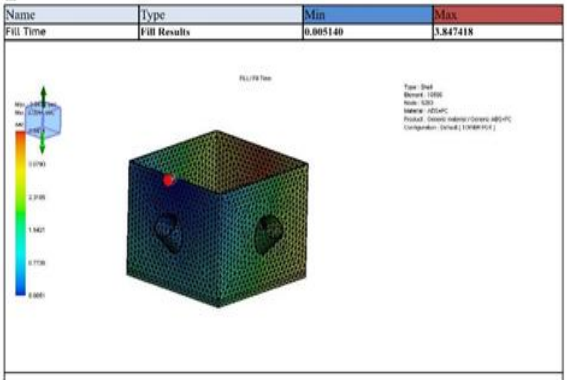

Fig. 3.2 shows the Fill time(Top Left)

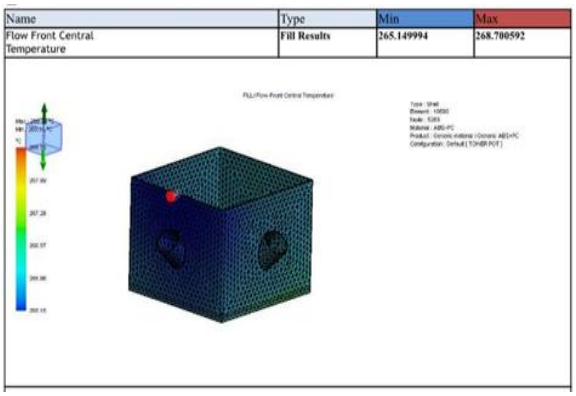

Fig. 3.3 shows the Flow Front Central Temperature (Bottom Left)

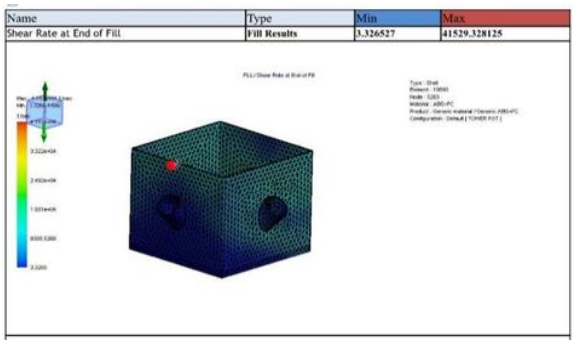

Fig. 3.4 shows the Shear Rate at end of Fill (Bottom Right)

3.2 Packing Phase Analysis

The packing stage ensures dimensional stability by compensating for shrinkage and maintaining cavity pressure.

(i) Volumetric Shrinkage: Volumetric shrinkage at the end of packing is shown in Fig. 3.5, with values from 2.48% to 5.56%. These values fall within typical shrinkage limits for ABS. However, areas with >5% shrinkage may be prone to warping or internal void formation, indicating that packing pressure or holding time should be fine-tuned.

(ii) Shear Rate at End of Packing: The shear rate distribution during the packing cycle. Fig. 3.6 shows significantly reduced values between 0.0085 s^{-1} and 21.51 s^{-1}. The reduced shear activity is desirable, as it indicates stable material consolidation without excessive internal friction or flow-induced stresses.

(iii) Pressure at End of Packing: The packing pressure distribution in Fig. 3.7 ranges from 13.14 MPa to 29.84 MPa. Moderate and uniform packing pressure suggests effective void reduction and strong material compaction. The relatively narrow pressure range ensures good dimensional accuracy and mechanical reliability.

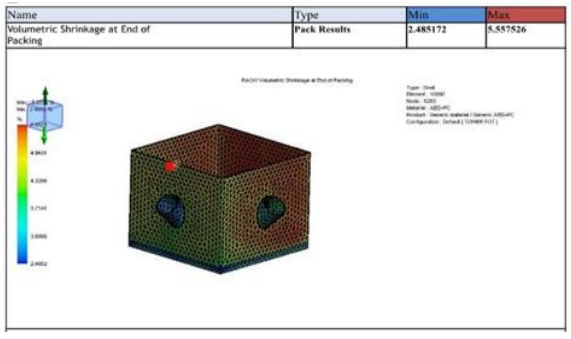

Fig. 3.5 shows the Volumetric Shrinkage at End of Packing (Left)

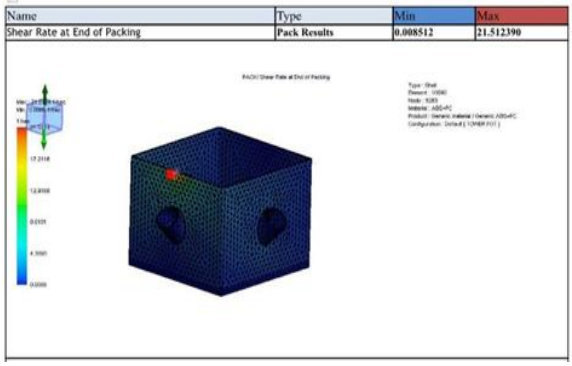

Fig. 3.6 shows the Shear Rate at End of Packing (Top Right)

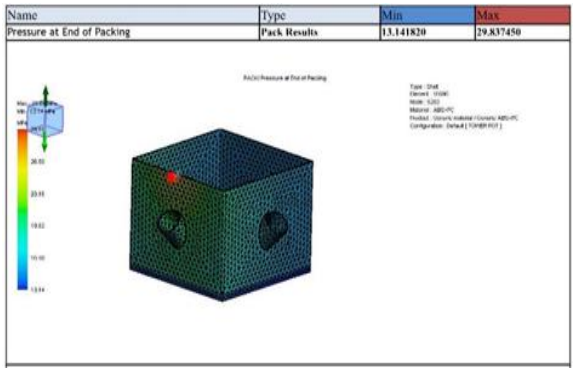

Fig. 3.7 shows the Pressure at End of Packing (Bottom Right)

3.3 Injection Pressure Profile

The maximum injection pressure values are summarized in Table 3.1, and the corresponding pressure-time graph is shown in Fig. 3.8. Pressure rises sharply during the first 5 seconds, reaching 70 MPa during the cavity-filling stage. A gradual decline in pressure marks the packing phase, during which additional material compensates for shrinkage. After 10 seconds, pressure drops significantly, indicating the start of the cooling phase.

The graph clearly delineates the injection, packing, and cooling phases. This behavior reflects an efficient flow cycle with stable packing and controlled cooling essential for precision components.

Table 3.1 shows the Maximum Injection Pressure data

Name	Type	Min	Max
Max.Injection Pressure	X-Y Plot	0.000000	74.59002

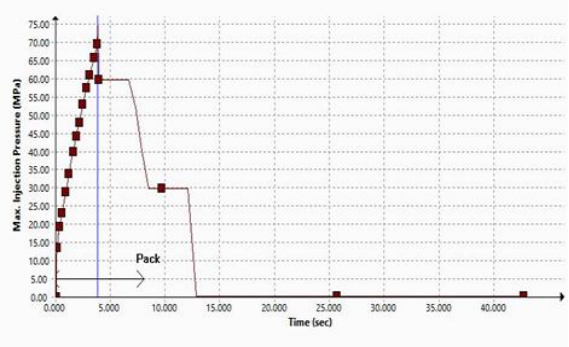

Fig. 3.8 shows the plot of Injection Pressure

3.4 Melt Front Flow Rate Profile

Table 3.2 summarizes the flow-rate range, while Fig. 3.9 illustrates the melt front flow-rate progression. Flow rate peaks around 600 cc/s within the first 5 seconds, aligning with rapid mold filling. A sharp drop follows as the process enters the packing stage. Flow rate stabilizes near zero through the cooling phase.

The peak and subsequent stabilizing behavior confirm proper cavity filling followed by controlled compression and cooling critical for maintaining structural integrity and avoiding flow-line defects.

Table 3.2 shows the Melt Front Flow Rate			
Name	Type	Min	Max
Melt Front Flow Rate	X-Y Plot	-6.918000	1668.73

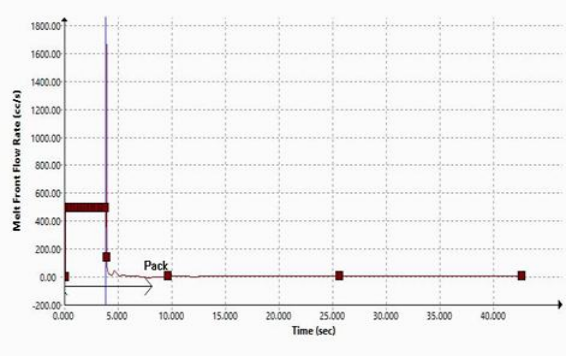

Fig. 3.9 shows the plot of Melt Front Flow Rate

IV. CONCLUSIONS

Based on the topology-optimized design evaluation and the detailed injection molding simulation results, the following conclusions are drawn:

The injection phase exhibited significantly high-pressure requirements, with the peak pressure reaching 74.6 MPa. Although this value remains within the allowable operational limits, it approaches the upper safety threshold, indicating potential pressure–flow inefficiencies in the current mold layout. Such behavior suggests the need for further optimization of gate dimensions, runner design, or flow-channel architecture to reduce unnecessary pressure buildup. Additionally, the filling pattern was highly non-uniform, with fill times ranging from 0.0051 seconds to 3.847 seconds. This substantial variation indicates the presence of flow imbalance and potential hesitation zones that could compromise part integrity, surface finish, and overall consistency of the molded component.

Flow-front temperature remained relatively stable throughout most of the filling stage, which helps minimize thermal degradation and preserves material performance. However, the temperature exceeded the recommended upper limit by nearly 30°C at the end of fill, raising concerns about burn-mark formation, polymer degradation, and localized stress concentrations arising from high shear heating. These concerns are further reinforced by the excessive shear-rate levels recorded during the process, reaching as high as 41,529 s^{-1}. Such extreme shear conditions can induce polymer chain scission, unwanted molecular orientation, and subsequent warpage, highlighting the need for controlled flow velocity and smoother internal flow passages.

The packing phase revealed volumetric shrinkage values within acceptable ranges but displayed noticeable non-uniformity, with shrinkage varying from 2.48% to 5.55%. This variation is likely to produce localized deformation and dimensional inaccuracies during cooling. While the overall packing pressures, ranging between 13.14 MPa and 29.83 MPa, fall within the required operational limits, the inconsistency in pressure distribution implies that certain regions of the cavity may not be receiving adequate compensatory pressure. This can lead to internal voids, density variations, and an overall reduction in structural uniformity.

Cooling behavior also warrants refinement, as elevated end-of-fill temperatures combined with uneven shrinkage can generate thermal stresses, differential contraction, and warpage during the cooling and ejection stages. Improvements in thermal management particularly through optimized cooling-channel layout and more uniform mold-surface

temperature control could significantly enhance structural reliability and reduce defect formation. Moreover, moderate reductions in injection speed and pressure may help stabilize the flow front, reduce excessive shear rates, and mitigate defects associated with thermal or shear-induced stresses.

Finally, adjustments to packing pressure and holding time are essential for achieving more uniform shrinkage and improving dimensional stability, especially for complex or topology-optimized components. Such refinements will contribute to minimizing warpage, improving structural accuracy, and ensuring consistent part quality across varying geometries.

REFERENCES

[1] D. R. Hershey, "Solution culture hydroponics: History & inexpensive equipment," The American Biology Teacher, vol. 56, no. 2, pp. 111–118, 1994.

[2] M. D. Mamta, "A review on plant without soil Hydroponics," International Journal of Research in Engineering and Technology, vol. 2, no. 3, pp. 299–304, 2013.

[3] M. J. Dos Santos, "Smart cities and urban areas: Aquaponics as innovative urban agriculture," Urban Forestry & Urban Greening, vol. 20, pp. 402–406, 2016.

[4] I. A. Lakhiar, J. Gao, T. N. Syed, F. A. Chandio, and N. A. Buttar, "Modern plant cultivation technologies in agriculture under controlled environment: A review on aeroponics," Journal of Plant Interactions, vol. 13, no. 1, pp. 338–352, 2018.

[5] J. E. Rakocy, M. P. Masser, and T. M. Losordo, "Recirculating aquaculture tank production systems: Aquaponics Integrating fish and plant culture," SRAC Publication, no. 454, pp. 1–16, 2006.

[6] B. M. Eldridge et al., "Getting to the roots of aeroponic indoor farming," New Phytologist, vol. 228, no. 4, pp. 1183–1192, 2020.

[7] G. Kim and S. Kim, "Evaluation of the environmental sustainability of 3D-printed hydroponics," Sustainability, vol. 11, no. 17, p. 4758, 2019.

[8] Y. Cheng and C. Hsiao, "Design and manufacturing of aeroponic systems using 3D printing technology," in Advances in Manufacturing Technology XXXI, pp. 117–122, 2017.

[9] Y. Takeuchi, "Printable hydroponics: Digital fabrication of ecological systems," in Proc. ISS, 2018, pp. 433–435.

[10] I. Hager, A. Golonka, and R. Putanowicz, "3D printing of buildings and building components as the future of sustainable construction?," Procedia Engineering, vol. 151, pp. 292–299, 2016.

[11] D. D. Le and H. K. Lee, "3D-printed aeroponic tower for vertical farming: A feasibility study," Sustainability, vol. 11, no. 23, p. 6608, 2019.

[12] G. Narayana, R. Gopi, and G. Shilpashree, "Design and development of a vertical hydroponic farming tower," in Proc. IEEE 4th Int. Conf. IoT in Social, Mobile, Analytics and Cloud, 2020.

[13] J. T. Kate, G. Smit, and P. Breedveld, "3D-printed upper limb prostheses: A review," Disability and Rehabilitation: Assistive Technology, vol. 12, pp. 300–314, 2017.

[14] I. Nir, "Growing plants in aeroponic growth system," Acta Horticulturae, no. 126, pp. 435–448, 1982.

[15] B. Khoshnevis, "Automated construction by contour crafting Related robotics and information technologies," Automation in Construction, vol. 13, no. 1, pp. 5–19, 2004.

[16] C. Mandrycky, A. Wang, K. Kim, and D.-H. Kim, "3D bioprinting for engineering complex tissues," Biotechnology Advances, vol. 34, no. 4, pp. 422–434, 2016.

[17] S. H. Baek, J. S. Song, and M. S. Kim, "Structural analysis and design optimization of 3D-printed modular hydroponic systems," Journal of Agricultural Engineering Research, vol. 123, pp. 45–58, 2016.

[18] Y. Takeuchi, "Printable hydroponic gardens: Initial explorations and considerations," in Extended Abstracts of CHI 2016 (alt.chi), pp. 449–458.

[19] B. Khoshnevis, D. Hwang, K. T. Yao, and Z. Yeh, "Mega-scale fabrication by contour crafting," International Journal of Industrial and Systems Engineering, vol. 1, no. 3, pp. 301–320, 2006.

[20] J. Woodhouse and M. S. Johnson, “Effect of superabsorbent polymers on survival and growth of crop seedlings,” Agricultural Water Management, vol. 20, no. 1, pp. 63–70, 1991.

[21] J. Liu, Z. Li, L. Wang, and O. Sigmund, “Design for additive manufacturing with topology optimization: A review,” Additive Manufacturing, vol. 21, pp. 584–604, 2018.

[22] S. Raut, V. S. Jatti, N. K. Khedkar, and N. R. Banapurmath, “Investigation of the effect of built orientation on mechanical properties and total cost of FDM parts,” Rapid Prototyping Journal, vol. 20, no. 3, pp. 175–185, 2014.

[23] K. Szykiedans and W. Credo, “Mechanical properties of FDM and SLA low-cost 3D prints,” MMS Conference Proceedings, vol. 19, no. 5, pp. 283–296, 2015.